

Unconventional Quantum Critical Phenomena in $(\text{Sr}_{1-x}\text{Ca}_x)_3\text{Ru}_2\text{O}_7$

Z. Qu¹, L. Spinu², V. Dobrosavljevic³, W. Bao⁴, J.W. Lynn⁵, J. Peng¹, T.J. Liu¹, D. Fobes¹, E. Flesch¹, and Z.Q. Mao^{1*}

¹ *Physics Department, Tulane University, New Orleans, Louisiana 70118, USA.*

² *AMRI and Physics Department, University of New Orleans, Louisiana 70148, USA.*

³ *Department of Physics and MHFML, Florida State University, Tallahassee, Florida 32306, USA*

⁴ *Los Alamos National Laboratory, Los Alamos, New Mexico 87545, USA.*

⁵ *NIST Center for Neutron Research, National Institute of Standards and Technology, Gaithersburg, Maryland 20899, USA*

In this letter, we report disorder-induced unconventional quantum critical behaviors in $(\text{Sr}_{1-x}\text{Ca}_x)_3\text{Ru}_2\text{O}_7$ ($0 \leq x \leq 1$). We discovered a quantum phase which obeys a new phenomenological scaling expression derived by extending the quantum Griffiths model; this phase freezes into a ferromagnetic cluster glass phase when the temperature is low enough. These results offer a rare opportunity to test theories of quantum phase transitions in disordered metallic systems.

PACS number(s): 73.43.Nq, 75.40.-s, 75.30.Kz, 71.27.+a.

A Quantum phase transition (QPT) occurs when competing interactions in a system are tuned such that the transition to long range order is suppressed to zero temperature. The physical properties of many systems of current interest, such as unconventional forms of superconductivity and magnetism, and anomalous non-Fermi-liquid (FL) behavior, are thought to be controlled over wide thermodynamic ranges by QPTs.¹⁻⁴ Theoretical work⁵⁻¹¹

suggests that QPTs can be strongly affected by disorder, leading to dramatic, non-perturbative effects, e.g., quantum Griffiths phenomena.^{6,9,10} However, few experimental results are available for comparison with the theory. Here we report the observation of disorder-induced unconventional quantum critical behaviors in $(\text{Sr}_{1-x}\text{Ca}_x)_3\text{Ru}_2\text{O}_7$, where we discovered a quantum phase obeying a new phenomenological scaling expression derived by extending the quantum Griffiths model.

$(\text{Sr}_{1-x}\text{Ca}_x)_3\text{Ru}_2\text{O}_7$ is the $n = 2$ member of the Ruddlesden-Popper series of ruthenates; both end members, $\text{Sr}_3\text{Ru}_2\text{O}_7$ and $\text{Ca}_3\text{Ru}_2\text{O}_7$, have been extensively studied and show fascinating properties. $\text{Sr}_3\text{Ru}_2\text{O}_7$ has a paramagnetic (PM) FL ground state.¹² Moderate magnetic fields induce a metamagnetic QPT in this material; non-FL behavior and a nematic liquid phase near the critical point, have also been reported.^{13,14} In contrast, $\text{Ca}_3\text{Ru}_2\text{O}_7$ exhibits an antiferromagnetic (AFM) ordering at 56K, followed by a first-order structural transition at 48 K,^{15,16} which leads to orbital ordering¹⁷ and an incomplete Mott-insulator transition¹⁸; Moreover, giant magnetoresistance was observed and attributed to a bulk spin-valve effect.^{16,19} Given the rich physics in both ends, $(\text{Sr}_{1-x}\text{Ca}_x)_3\text{Ru}_2\text{O}_7$ solid solution is expected to be interesting. Previous studies on polycrystals and flux-grown single crystals of this system suggest that an unusual phase might occur near $x \sim 0.3$.²⁰⁻²²

We have recently succeeded in growing super-clean single crystals of $(\text{Sr}_{1-x}\text{Ca}_x)_3\text{Ru}_2\text{O}_7$ ($0 \leq x \leq 1$) using a floating-zone technique, and have established a phase diagram for this system through magnetization, specific heat, resistivity, and neutron scattering measurements. As shown in Fig. 1, the phase diagram consists of the following five regions at low temperatures: (I) Long-range AFM state for $1 \geq x \geq 0.40$. (II) Itinerant metamagnetic state near the Sr side for $0.08 > x \geq 0$. (III) PM state for $0.15 > x \geq 0.08$, accompanied by non-FL behaviors. (IV) Unusual ferromagnetic (FM) cluster glass (CG) phase for $0.40 > x > 0.15$, featured by an extremely large Wilson ratio ~ 120 . (V) Modified

quantum Griffiths phase, which occurs above the CG phase and follow a new scaling expression obtained by phenomenologically extending the quantum Griffiths phase model.

Figure 2 shows the magnetization data of typical samples. For the samples in the AFM phase region, two successive transitions, respectively corresponding to the AFM and structure transition, can clearly be identified. With partial Sr substitution for Ca, the Néel temperature T_N shows a slight increase and then a gradual decrease after reaching a maximum at $x = 0.9$, while the structural transition temperature T_{ST} is continuously suppressed until $x = 0.4$. Specific heat measurements reveal that the structural phase transition changes from a first-order type for $0.9 < x \leq 1$ to a second-order type for $0.4 < x < 0.9$ (data not shown). Our observation of suppression of T_N and T_{ST} caused by Sr substitution for Ca is consistent with previous results obtained on polycrystalline and flux-grown single crystal samples.^{20, 21}

For pure $\text{Ca}_3\text{Ru}_2\text{O}_7$, we performed elastic neutron scattering measurements. A set of magnetic Bragg peaks of $(0kl)$ with $k = 0, 2$ and $l = 1, 3, 5, \dots, 11$ were measured. The magnetic structure determined from these data is displayed in the inset of Fig. 1, which shows that the FM RuO_2 bilayers stack antiferromagnetically along the c axis. This result is consistent with the magnetic structure previously proposed based on one powder neutron diffraction peak (001) ,¹⁵ which did not allow a determination of the magnetic moment and its direction. The analysis of our data reveals that the magnitude of moment is $1.86 \pm 0.02 \mu_B$ per Ru at 2K with the direction along the b -axis, indicating a nearly fully polarized state for the RuO_2 bilayers.

When the Ca content is reduced below 40%, the AFM ordering disappears and M/H shows paramagnetic behavior, as shown in Fig. 2. $\text{Sr}_3\text{Ru}_2\text{O}_7$ exhibits behavior similar to data previously reported;^{12, 13} it shows a peak around 16K (T_{\max}) in $\chi(T)$ and a metamagnetic transition at ~ 5 T for $H//ab$ (see Inset **a** in Fig. 2). Both features are suppressed by partial Ca substitution for Sr and disappear for $x > 0.08$. Another striking feature is that the M/H at

temperatures below 10 K enhances drastically with increasing Ca content. The concave $M(H)$ curves (Inset **a** in Fig. 2), as well as the hysteresis seen in the field sweep measurements (not shown), indicate that the increase in M/H of these samples at low temperatures originates from enhanced FM fluctuations. Furthermore, samples close to $x = 0.3$ have an extremely large Wilson ratio $R_W = (\pi^2 k_B^2 / 3\mu_B^2)(\chi / \gamma_e) \sim 120$ where χ is electronic specific heat coefficient (see Inset **d** in Fig. 2), suggesting that the system is driven to a state very close to a 2-D FM instability. This behaviour is quite similar to the Ca doping effect in the $\text{Ca}_{2-x}\text{Sr}_x\text{RuO}_4$ system.^{23, 24} Our observation of magnetic properties for samples with $x < 0.4$ is very different from early results obtained on flux-grown crystals for which the magnetic ground states were claimed to be long-range FM with $T_c \sim 100$ K for $x = 0$.²¹ The FM phase in those samples is most likely due to intergrowth of the trilayered phase $(\text{Sr,Ca})_4\text{Ru}_3\text{O}_{10}$ which is FM with $T_c \approx 100$ K.²⁵

To further characterize the magnetic ground state of the phase between the AFM and metamagnetic state in the phase diagram, we measured the susceptibility $\chi(T)$ under 50 Oe with field-cooling (FC) and zero-field-cooling (ZFC) histories for samples with $x < 0.40$. $\chi(T)$ exhibits irreversibility between ZFC and FC for $0.15 < x < 0.4$; the typical data are shown in Inset **b** in Fig. 2. This fact, together with the frequency dependence of the peak in ac susceptibility (Inset **c** in Fig. 2), indicate that the samples in the $0.15 < x < 0.4$ range have glassy ground states, similar to the behavior observed in $\text{Ca}_{2-x}\text{Sr}_x\text{RuO}_4$.²⁴ Since the samples in the range of $0.15 < x < 0.4$ are close to a 2-D FM instability, this glassy state should be a FM CG.

Since this FM CG phase occurs in the vicinity of AFM long-range order, one may ask whether the PM states close to the CG phase exhibit quantum critical behavior. Previous angle-resolved photoemission measurements on flux-grown crystals reveal a qualitative

change of electronic properties near $x \sim 0.3\text{-}0.4$, which is suggested to be associated with a QPT.²² Given that Ca^{2+} substitution for Sr^{2+} in $(\text{Sr}_{1-x}\text{Ca}_x)_3\text{Ru}_2\text{O}_7$ introduces substantial disorder into the system, quantum critical fluctuations might lead to exhibit unconventional properties, e.g., quantum Griffiths phenomena as mentioned above, if they indeed exist and strongly interplay with disorder. The quantum Griffiths model indicates that in the vicinity of the QPT of a disordered system there may exist some arbitrary regions which are devoid of disorder and can develop local order.^{9,10} These regions show slow dynamics with their energy scales following a power law distribution, which leads to anomalous power law singularities in thermodynamic properties, i.e., $\chi(T) \sim T^{\alpha-1}$, $C(T)/T \sim T^{\alpha-1}$, $M(T=0\text{K}) \sim H^\alpha$ with $0 < \alpha < 1$.⁹ Moreover, the magnetization is expected to follow a scaling law of $M(H,T) \sim H^\alpha f(x)$ where $f(x = H/T)$ is the scaling function^{13,14}. Recent work suggests that if spin fluctuations due to the long-range Ruderman-Kittel-Kasuya-Yosida (RKKY) interactions are taken into account, the quantum Griffiths phase is destabilized and a CG phase forms at low temperature.¹¹

If the CG phase we observed in $(\text{Sr}_{1-x}\text{Ca}_x)_3\text{Ru}_2\text{O}_7$ is truly relevant to this theoretically predicted one, we might expect to observe unconventional features relevant to the quantum Griffiths phenomena. We have examined our data with the standard quantum Griffiths model and found that this model is applicable only qualitatively. As shown in the insets of Fig. 3, $\chi(T)$ indeed shows a power law temperature dependence in the low temperature range above the frozen temperature of the CG phase T_f ; the $M(H)$ curve at a finite temperature displays a crossover from linearity to power law behavior, and the crossover field H^* shifts toward zero with decreasing temperature. All these features are consistent with the power law singularities of the quantum Griffiths phenomena. Nevertheless, the value of α extracted from $\chi(T)$ is negative, which is not in the expected range of $0 < \alpha < 1$ for the quantum Griffiths model^{9,10} (e.g. $\alpha = -1.1$ for $x = 0.3$), and is also inconsistent with the α derived from

the $M(H) \sim H^\alpha$ at high fields (e.g. $\alpha = 0.33$ for $x = 0.3$). Moreover, the $M(H,T)$ data were not found to follow the expected scaling law.

This quantitative inconsistency might be due to the simplicity of the quantum Griffiths model where one assumes that each droplet is in a fully ordered state with a temperature-independent magnetization.^{9, 10} We note that $\chi(T) \sim T^{\alpha-1}$ with $\alpha < 0$, which is observed in our system, corresponds to a spin susceptibility that grows faster than that of free spins; this implies that the magnetic moment within a given droplet must be temperature dependent, which seems quite possible given that our samples in the $0.15 < x < 0.4$ range are so close to a FM instability. Therefore, we propose a new scaling expression $M(H,T) \sim H^\alpha F(x)$ where $F(x=H/H^*(T))$ is the scaling function. Given that $M(H)$ shows a linear power law crossover, analytically we have $\chi(T)H^* = AH^{*\alpha}$ at the crossover field H^* . If $\chi(T)$ is expressed as $\chi(T) \sim T^{-\beta}$, we can derive $H^*(T) \sim T^\delta$ with $\delta = \beta/(1-\alpha)$. From our data, we find $H^* \sim T^\delta$ with $\delta > 1$ (e.g., $\delta = 3.13$ for $x = 0.3$), rather than $H^* \sim T$ assumed in the quantum Griffiths model.

We analyzed our $M(H,T)$ data with this extended scaling expression and found that the data amazingly collapse in a temperature range above T_f for a given sample in the $0.15 < x < 0.4$ range, as shown in Fig. 3. The maximum temperature T_{scaling} , above which the scaling behavior breaks down, varies systematically with Ca content, as shown in Fig. 1. Surprisingly, $T_{\text{scaling}}(x)$ appears to follow the extrapolation of $T_N(x)$. All these characteristics strongly suggest that the PM phase right above the CG phase is relevant to the quantum Griffiths phenomena, which we define as a modified quantum Griffiths phase.

We also observe non-FL behaviors from specific heat and electric transport measurements for the PM states close to the CG phase. As shown in Fig. 4a, the electronic

specific heat divided by temperature C_e/T exhibits an upturn anomaly at low temperatures for $0.08 < x < 0.40$, in sharp contrast with the constant behavior of FL ground state. The tendency of approaching saturation below 3 K for $0.15 < x < 0.4$ is clearly due to the formation of the CG phase, which reduces the electronic specific heat. For the 10% sample, C_e/T appears linear below 6K on the $\log T$ scale. However, plotted on a double log scale, C_e/T also looks linear within a narrower temperature range, which means that here it is almost indiscernible between logarithmic and power law singularities. Additionally, the variation of γ_e , χ and R_W with the Ca content show a broad peak near $x \sim 0.3$, rather than a divergence (see Inset **d** in Fig. 2), consistent with the theoretically predicted “rounding” of QPTs in the presence of disorder.⁸

Figure 4**b-d** show resistivity data for the samples with $0 \leq x < 0.4$. From Fig. 4**b**, it can be seen that the FL temperature is quickly suppressed by Ca substitution, down to below 1 K by 5% Ca. For samples with x close to 0.1-0.15, $\rho(T)_{ab}$ shows a temperature dependence close to $T^{4/3}$ for $6 \text{ K} < T < 12 \text{ K}$ (see Inset in Fig. 4**b**), then crossovers to $T^{2.5-3.0}$ dependence for $T < 2 \text{ K}$. The $T^{4/3}$ dependence seems consistent with the expected non-FL behavior caused by quantum fluctuations near a 2D FM instability,³ while the $T^{2.5-3.0}$ dependence below 2K could be ascribed to increased spin scattering due to close proximity to the FM CG phase. As seen in Fig. 4**c** and 4**d**, when the Ca content is close to 30%, $\rho(T)_{ab}$ exhibits a non-metallic behavior for $T < T_f$, which can be tuned to quadratic temperature dependence with applied magnetic field, indicating that the spin scattering among FM clusters plays a critical role in the transport process. Spin-scattering among clusters should be much weaker than scattering from disorder induced by Ca/Sr substitutions since the variation of residual resistivity ρ_0 with the Ca content (Inset of Fig. 4**c**) can be fitted approximately with Nordheim’s law $\rho_0 = Ax(1-x)$ which is based on disorder scattering alone.

In summary, we established a phase diagram of magnetic states for the $(\text{Sr}_{1-x}\text{Ca}_x)_3\text{Ru}_2\text{O}_7$ system, in which disorder was found to have strong interplay with the quantum critical fluctuations tuned by the Ca/Sr substitution. We discovered a quantum phase obeying a new phenomenological scaling expression derived by extending the quantum Griffiths model. Although the microscopic mechanism of this scaling behavior is yet to be clarified, it places an additional constraint on further theory in this area.

We thank C.M. Varma, I. Vekhter, A.V. Balatsky, M.J. Case, Z. Islam, Y. Liu and H.Q. Yuan for useful discussion. This material is based upon work at Tulane supported by NSF under grant DMR-0645305 and by DOE under DE-FG02-07ER46358 and the Research Corporation, and work at UNO supported by DARPA through Grant No. HR0011-07-1-0031, and work in Florida supported by NSF under grant DMR-0542026, and work at LANL supported by DOE. Identification of commercial equipment is not intended to imply recommendation or endorsement by NIST.

*Electronic address: zmao@tulane.edu

1. S. Sachdev, *Quantum phase transitions* (Cambridge Univ. Press, Cambridge, 1999).
2. S.L. Sondhi, S.M. Girvin, J.P. Carini, and D. Shahar, Rev. Mod. Phys. **69**, 315 (1997).
3. G.R. Stewart, Rev. Mod. Phys. **73**, 797 (2001).
4. H.v. Löhneysen, A. Rosch, M. Vojta, and P. Wölfle, Rev. Mod. Phys. in the press.
5. D.S. Fisher, Phys. Rev. Lett. **69**, 534 (1992).
6. A.H. Castro Neto, G. Castilla, and B.A. Jones, Phys. Rev. Lett. **81**, 3531 (1998).
7. A.J. Millis, D.K. Morr, and J. Schmalian, Phys. Rev. Lett. **87**, 167202 (2001).
8. T. Vojta, Phys. Rev. Lett. **90**, 107202 (2003).
9. E. Miranda, and V. Dobrosavljević, Rep. Prog. Phys. **68**, 2337 (2005).
10. T. Vojta, J. Phys. A **39**, R143 (2006).

11. V. Dobrosavljević, and E. Miranda, *Phys. Rev. Lett.* **94**, 187203 (2005).
12. S.I. Ikeda, Y. Maeno, S. Nakatsuji, M. Kosaka, and Y. Uwatoko, *Phys. Rev. B* **62**, R6089 (2000).
13. S.A. Grigera, *et al.* *Science* **294**, 329 (2001).
14. R.A. Borzi, *et al.* *Science* **315**, 214 (2007).
15. Y. Yoshida, *et al.* *Phys. Rev. B* **72**, 054412 (2005).
16. G. Cao, *et al.* *Phys. Rev. B* **67**, 060406(R) (2003).
17. J.F. Karpus, R. Gupta, H. Barath, S.L. Cooper, and G. Cao, *Phys. Rev. Lett.* **93**, 167205 (2004).
18. F. Baumberger, *et al.* *Phys. Rev. Lett.* **96**, 107601 (2006).
19. D.J. Singh, and S. Auluck, *Phys. Rev. Lett.* **96**, 097203 (2006).
20. S. Ikeda, Y. Maeno, and T. Fujita, *Phys. Rev. B* **57**, 978 (1998).
21. G. Cao, S.C. McCall, J.E. Crow, and R.P. Guertin, *Phys. Rev. B* **56**, 5387 (1997).
22. A.V. Puchkov, *et al.* *Phys. Rev. Lett.* **81**, 2747 (1998).
23. S. Nakatsuji, and Y. Maeno, *Phys. Rev. Lett.* **84**, 2666 (2000).
24. S. Nakatsuji, *et al.* *Phys. Rev. Lett.* **90**, 137202 (2003).
25. S. Chikara, *et al.* *Phys. Rev. B* **73**, 224420 (2006).

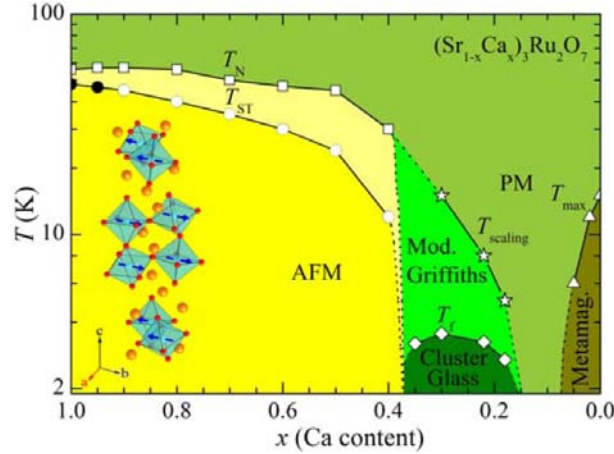


Figure 1: Magnetic phase diagram of $(\text{Sr}_{1-x}\text{Ca}_x)_3\text{Ru}_2\text{O}_7$. AFM: antiferromagnetic phase; T_N : Néel temperature; T_{ST} : structural phase transition temperature. The closed and open circles represent first and second order structural transition respectively. Metamag.: itinerant metamagnetic state; T_{max} : temperature of the peak in the susceptibility, below which the metamagnetic transition occurs. PM: paramagnetic state. T_f : frozen temperature of the CG phase. Mod. Griffiths: a modified quantum Griffiths phase (see the text). T_{scaling} is the maximum temperature for the scaling behavior of magnetization. Inset: magnetic structure of $\text{Ca}_3\text{Ru}_2\text{O}_7$ determined by neutron scattering.

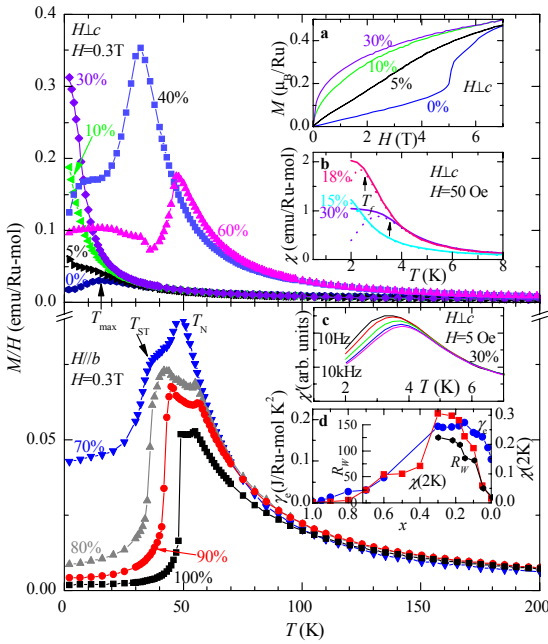


Figure 2: Magnetic properties for $(\text{Sr}_{1-x}\text{Ca}_x)_3\text{Ru}_2\text{O}_7$. Inset **a**: M vs. H at 2 K. Inset **b**: $\chi(T)$ measured at 50 Oe with FC (solid lines) and ZFC (dotted lines) histories. The temperature where irreversibility occurs is defined as the frozen temperature T_f of the CG phase. Inset **c**: ac susceptibility measured at various frequencies. Inset **d**: χ at 2K and 0.3T, χ , and Wilson ratio vs. the Ca content.

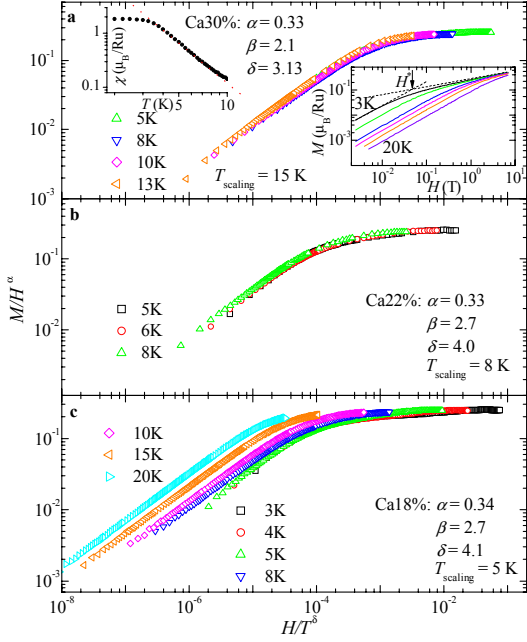


Figure 3: Scaling plot of $M/H^\alpha \sim H/T^\delta$ for $(\text{Sr}_{1-x}\text{Ca}_x)_3\text{Ru}_2\text{O}_7$. Insets in (a): $\chi(T)$ and $M(H, T)$ data for $x = 0.3$ on double-log scales. The intersection of the linear extrapolations of the $M(H)$ curves at low and high fields is defined as the crossover field H^* . α is determined from $M(H) \sim H^\alpha$ at high fields and β is determined from $\chi(T) \sim T^{-\beta}$ within the low temperature region right above T_f . $\delta = \beta/(1-\alpha)$ (see the text). T_{scaling} is the maximum temperature for the scaling behaviour.

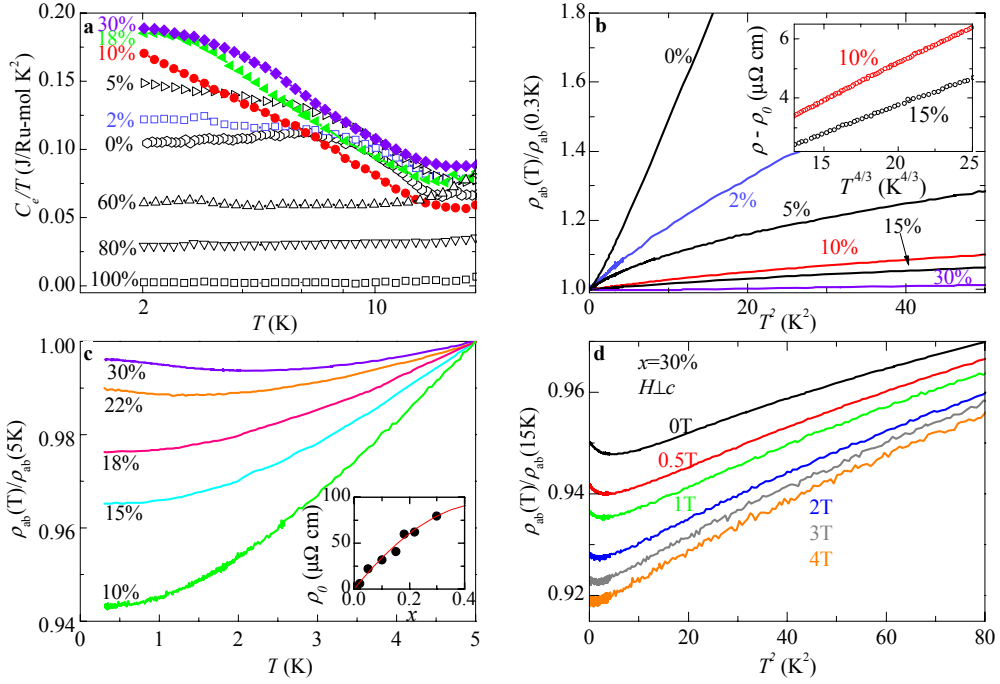


Figure 4: **a.** Electronic specific heat divided by temperature C_e/T as a function of T for $(\text{Sr}_{1-x}\text{Ca}_x)_3\text{Ru}_2\text{O}_7$, plotted on a $\log T$ scale. **b.** Normalized in-plane resistivity $\rho(T)_{ab}$ vs. T^2 ; inset: $\rho(T)_{ab}$ subtracted by residual resistivity ρ_0 plotted on a $T^{4/3}$ scale for samples with $x = 0.10$ and 0.15 . **c.** Normalized $\rho(T)_{ab}$ vs. T ; inset: the residual resistivity vs. Ca content for $x < 0.4$. The red solid line represents a fit to the Nordheim formula with $A = 378 \mu\Omega \text{ cm}$. **d.** Normalized $\rho(T)_{ab}$ at various magnetic fields for the sample with $x = 0.30$.